Forward-looking Assimilation of MODIS-derived Snow Covered Area into a Land Surface Model

Benjamin F. Zaitchik*, Earth System Science Interdisciplinary Center, University of Maryland College Park & Hydrological Sciences Branch, NASA Goddard Space Flight Center

Matthew Rodell, Hydrological Sciences Branch, NASA Goddard Space Flight Center

*Corresponding author's address:

Hydrological Sciences Branch, Code 614.3

NASA Goddard Space Flight Center

Greenbelt, MD 20771

ben.zaitchik@nasa.gov

Abstract

Snow cover over land has a significant impact on the surface radiation budget, turbulent energy fluxes to the atmosphere, and local hydrological fluxes. For this reason, inaccuracies in the representation of snow covered area (SCA) within a land surface model (LSM) can lead to substantial errors in both offline and coupled simulations. Data assimilation algorithms have the potential to address this problem. However, the assimilation of SCA observations is complicated by an information deficit in the observation—SCA indicates only the presence or absence of snow, and not snow volume—and by the fact that assimilated SCA observations can introduce inconsistencies with atmospheric forcing data, leading to non-physical artifacts in the local water balance. In this paper we present a novel assimilation algorithm that introduces MODIS SCA observations to the Noah LSM in global, uncoupled simulations. The algorithm utilizes observations from up to 72 hours ahead of the model simulation in order to correct against emerging errors in the simulation of snow cover while preserving the local hydrologic balance. This is accomplished by using future snow observations to adjust air temperature and, when necessary, precipitation within the LSM. In global, offline integrations, this new assimilation algorithm provided improved simulation of SCA and snow water equivalent relative to open loop integrations and integrations that used an earlier SCA assimilation algorithm. These improvements, in turn, influenced the simulation of surface water and energy fluxes both during the snow season and, in some regions, on into the following spring.

1

1. Introduction

Average monthly snow cover in the Northern Hemisphere varies from 7% of all land area to more than 40%, making snow cover the fastest varying large-scale surface feature on Earth (Chang et al. 1990; Hall 1988). This variability has a dramatic impact on surface moisture and energy fluxes. Snow insulates the ground beneath, moderating soil temperatures during winter (Decker et al. 2003). Due to its high albedo, snow significantly reduces the absorption of radiation at the land surface, restraining turbulent energy fluxes and lowering near-surface air temperature (Baker et al. 1992; Liston 2004). In high latitude and high altitude regions, snow plays a dominant role in the local and regional hydrologic balance, with associated impacts on soil moisture, aquifer recharge, and vegetation growth (Flerchinger et al. 1994; Marsh 1999; Ren et al. 2007). Moreover, it is now understood that snow's influence on local energy fluxes has remote impacts, modifying atmospheric temperature and circulations on the regional scale (Elguindi et al. 2005; Ellis and Leathers 1999; Zaitchik et al. 2007) and climate dynamics on the continental to hemispheric scale (Bamzai and Shukla 1999; Cohen and Entekhabi 2001; Dery et al. 2005).

Given these significant effects, it is critical that models used in seasonal forecasts and retrospective climate studies accurately simulate the snow pack. For this reason, most modern land surface models (LSMs) include sophisticated snow routines designed to capture the accumulation, aging and melt of snow under a range of weather conditions (Ek et al. 2003; Roesch et al. 2001; Stieglitz et al. 2001; Takata et al. 2003). Unfortunately, even the most refined LSMs have difficulty capturing these processes over

an extended simulation (Foster et al. 1996; Pitman 2003). In a sense, snow is an inherently difficult quantity to model: for large areas of the planet, accumulation and melt processes are sensitive to small changes in air temperature, radiation fluxes, or surface properties, yet the presence versus absence of snow will itself have a dramatic impact on these variables. This means that small uncertainties in parameterization or forcing data can trigger errors in snow cover that quickly cascade into larger inaccuracies in albedo, soil moisture, energy exchange, and atmospheric conditions. As these inaccuracies compound, the model "drifts," leading to severe reductions in skill on the seasonal timescale. For hydrologic applications, drift with respect to snow simulation is an even larger problem; in many regions, accurate simulation of the depth of the snow pack and timing of snow melt are the most important aspects of hydrological monitoring and prediction systems.

The MODerate Imaging Spectrometer (MODIS) instruments, on NASA's *Terra* and *Aqua* satellites, offer twice daily observations of snow covered area (SCA) at 500m resolution, with near-global coverage (Hall et al. 2002). The reliability of these observations is much greater than that of LSM predictions at a similar resolution, but the information contained in a MODIS observation is much less. The LSM simulation of the snow pack includes information on snow water equivalent (SWE), snow depth, and, in some models, time-variable snow density. The simulation is also continuous in space and time, at a user-specified resolution. MODIS contains no information on SWE or snow depth, can provide a maximum of two daylight observations per day, and frequently suffers from data gaps due to cloud cover. As the MODIS SCA product is derived from

information in the visible and near infrared portions of the electromagnetic spectrum, observations can only be obtained under clear-sky, daytime conditions.

Data assimilation (DA) algorithms attempt to utilize the information in such discontinuous observations by integrating them into a numerical model. The model provides spatial and temporal continuity as well as physically-based schemes that allow an observation of one quantity to inform predictions of other modeled variables. The observation system provides reliable, independent information on a variable that the model simulates imperfectly, preventing model drift and improving the accuracy of the simulation. Our hypothesis is that data assimilation is the most effective method for utilizing MODIS-derived measurements of snow cover in studies of climate and hydrology. Further, as LSMs are frequently employed in a coupled mode with atmospheric models, a MODIS SCA assimilation system can be used to improve the initialization of numerical forecasts, a powerful predictive application of MODIS-derived information.

In this study, MODIS observations of SCA were assimilated into the Noah LSM (Chen et al. 1996; Ek et al. 2003) in global, retrospective simulations at 0.25° resolution. Simulations were performed for two northern hemisphere snow seasons, September 2005 – June 2006 and September 2006 - June 2007. The results of two assimilation algorithms are presented. The first, a rule-based direct insertion scheme, is a refinement of a system first presented by Rodell and Houser (2004) [hereafter, RH04]. In this algorithm, MODIS SCA observations are assigned a SWE equivalent on the basis of land cover, and

this value is used to overwrite simulated SWE whenever there is a contradiction between model and observation. The second algorithm is a novel, physically-based assimilation update that uses MODIS SCA observations from up to 72 hours ahead of the simulation to adjust snow accumulation and melt processes. This allows for smooth updates of snow that attempt to preserve the local hydrologic balance while preventing unrealistic add/melt and remove/accumulate cycles that occur in standard snow assimilation schemes whenever observations are in conflict with atmospheric forcing data.

The remainder of the paper is structured as follows. Section 2 provides background on the Noah LSM, satellite-derived snow observations, and data assimilation. Section 3 gives details of image processing, validation data, and the assimilation scheme. Simulation results and evaluation are presented in Section 4. Section 5 contains conclusions.

2. Background

(a) Noah LSM

The Noah land surface model is an advanced 1-D column model that simulates soil temperature, skin temperature, soil moisture (frozen and liquid, in four soil layers), snow states, surface energy and hydrologic fluxes, and subsurface runoff (Chen et al. 1996). The model is currently supported by the National Centers for Environmental Prediction (NCEP) and is in active development (e.g.,Ek et al. 2003). It is widely used in operational and research applications, and can be run in either coupled or uncoupled mode. Noah employs finite-difference spatial discretization methods and a Crank-

Nicholson time-integration scheme to solve the governing equations of the physical processes of the soil-vegetation-snowpack medium.

Noah contains a one layer snow model that simulates snow water equivalent (SWE) as the residual of snowfall – (snowmelt + sublimation). Snowfall occurs whenever there is non-zero precipitation and air temperature is $\leq 0°C$. Melt occurs whenever there is net available energy within the snowpack. When melt occurs, some water is stored within the snowpack and excess water is removed as runoff. Snow covered area is diagnosed as a function of SWE using a generalized snow depletion curve:

$$SCA = \min\left[1 - \left(\exp\left(-\frac{\tau \cdot SWE}{SWE_{SCA=1.0}}\right) - \frac{SWE}{SWE_{SCA=1.0}}\exp(-\tau)\right), 1.0\right] \quad (\text{Eq. 1})$$

Where τ is the snow distribution shape parameter (currently set to 4.0) and $SWE_{SCA=1.0}$ is a land cover specific parameter that defines the minimum SWE required for full snow cover. Snow depth is solved on the basis of SWE and snow density. Snow density is itself a predicted field, and is a function of total SWE in the snowpack, a temperature and SWE-dependent compaction scheme, and air temperature whenever snowfall is active (Koren et al. 1999).

(b) Satellite-derived snow observations

Satellite-based snow detection algorithms can be divided into two general categories: those that attempt a direct measurement of SWE and those that produce estimates of

SCA. SWE algorithms take advantage of the fact that the diameter of snow grains falls

within the same size range as microwave radiation (Chang et al. 1987; Chang et al. 2005).

This means that snow scatters microwaves of different wavelengths with widely differing

efficiency, and that the difference in scattering between two or more microwave channels

can be used to estimate SWE. Algorithms founded on this principle have been used to

retrieve SWE from SSM/I, AMSR-E and other passive microwave sensors. All such

algorithms, however, are plagued by the fact that microwave scattering is sensitive to

snow grain size, phase changes within the snowpack, and the presence of liquid water on

the snow surface. While there has been considerable progress on the theory of SWE

retrieval from passive microwave sensors (e.g., Durand and Margulis 2006), these data

products are not yet ready for practical use in DA (Andreadis and Lettenmaier 2006),

particularly in global applications (Cordisco et al. 2006).

Detecting the presence or absence of snow is a simpler problem for remote sensing, and

several sensors currently offer acceptably accurate estimates of SCA over the globe

(Bitner et al. 2002; Brubaker et al. 2005). With respect to the two general goals of

assimilating observations of snow—to improve representation of (*a*) the surface energy

balance and (*b*) snow water reserves—the assimilation of estimated SCA offers the

potential to improve *a* in all regions of the globe and *b* only in locations with partial or

sporadic snow cover, or areas where there is substantial model error in the timing of the

initiation and final melt of the seasonal snow pack. This expectation follows from

analyses of *in situ* snow observing stations, which show strong correlations between SCA

and SWE during periods of accumulation and ablation, but weak correlations in the middle of the snow season, when SCA nears 100% in a snowy region (Gong et al. 2007).

SCA can be retrieved by passive microwave sensors, such as SSMI and AMSR-E, that provide measurements under both clear and cloudy conditions but have coarse spatial resolution (25km or more), and by sensors that use the visible and near-infrared (VNIR) portion of the spectrum. VNIR sensors cannot penetrate clouds, but they offer superior spatial resolution. MODIS, for example, can detect snow presence/absence at 500m resolution, which is more than adequate for most climate and many hydrological applications. MODIS was selected for this study on account of its high spatial resolution and general reliability. It is our expectation that DA routines can effectively interpolate between discontinuous measurements in time and space, but that it is more difficult to disaggregate a spatially coarse measurement or to extract useful information from an error-prone observation. Since our goal is to design an assimilation scheme that can be applied globally but also at resolutions finer than 25 km, MODIS was identified as the best available data source.

(c) Data assimilation

The guiding principle of DA is that an observation and a prediction can be combined such that the result contains less uncertainty than either input. Here, the predictions are provided by a physically-based numerical model of land surface processes. The model contributes a high resolution, spatially and temporally continuous first-guess approximation of the assimilated state (in this case, snow water equivalent), based on

8

numerical representations of physical processes and other relevant data. The observations provide an external check on model predictions, preventing drift and correcting the model with respect to essential state variables. Hence the data assimilation scheme enables both scientific understanding and observations to inform estimates of a given variable, as well as associated states and fluxes, while addressing the spatial and temporal limitations of the observing system.

The assimilation of a SCA observation presents some challenge because it provides only partial information on the model field that it is used to inform. A SCA observation contains no information on snow depth, snow density, or snow water equivalent, which will all be influenced by the assimilation update, and the physical link between SCA and these variables is inconsistent in space and time. An early season snowfall, for example, might coat 100% of the observation footprint with a very thin layer of snow, while springtime melt might leave behind deep piles of dense snow that cover only 30% of the footprint.

The relationship between SCA and SWE at a given location can be described using a contextual snow depletion curve (SDC), which relates SCA to SWE on the basis of prior information and ground measurements (e.g., Anderson 1973). Ideally, such a geographically-specific SDC is informed by local data on typical patterns of snow depth distribution (e.g., Andreadis and Lettenmaier 2006; Kolberg et al. 2006). As such data are not available globally, Liston (2004) proposed a dichotomous key that divides the world into nine SDC landscapes, allowing for some refinement to globally uniform SDCs

in the absence of local data. The key lacks the local specificity and spatial resolution of some regionally-specific SDCs, but it was shown to have a significant impact on the simulation of snow processes in a regional model. The Subgrid Snow Distribution (SSNOWD) model derived from this key could be implemented within the framework of many existing LSMs.

Another approach to SCA assimilation is to map SCA observations onto predicted variables in the LSM on the basis of cross-state covariance estimates. Andreadis & Lettenmaier (2006) applied an Ensemble Kalman Filter (EnKF) assimilation scheme that used SCA observations to directly update SWE, while Clark et al. (2006) demonstrated a more extensive EnKF scheme that mapped SCA observations to update SWE, soil moisture, and groundwater. Both studies showed promise in a watershed-scale, but the requirement for reliable cross-state covariance estimates and statistically robust observation error estimates currently preclude global application of the techniques (Clark et al. 2006).

Acknowledging the information deficit encountered by both regionally-specific SDC assimilation schemes and EnKF routines, RH04 proposed a simple, conservative rule-based assimilation scheme to link SCA observations to SWE. In their assimilation of MODIS SCA into the Mosaic LSM they implemented a rule in which a thin layer of SWE (5 mm) was applied to any model grid cell for which MODIS reported SCA was > 0.4 and the LSM had no snow cover. For cells with MODIS SCA < 0.1, all snow was removed from the grid cell. This simple approach can be applied globally with

reasonable confidence, and it requires no modification to the basic routines of the LSM. As our goal is a globally-applicable assimilation routine that can be applied to existing, operational versions of the Noah LSM, we use the RH04 algorithm as the starting point for the algorithm developed in this study.

The RH04 algorithm, like most SCA assimilation methods, suffers from the inherent sensitivity of a snow update to any inconsistencies that might exist between the SCA observation and forcing fields of air temperature and precipitation. This leads to two problems. First, SCA assimilation tends to be much more effective at removing snow than adding snow. This is because model errors that increase SCA are the product of episodic snowfall events, and these events can be quickly counter-acted by a single snow free observation. Snow melt, on the other hand, can occur continuously as a function of air temperature. The assimilation of a SCA observation that adds SWE to a grid cell is subject to immediate melt if air temperature is above the freezing point. If added snow cover is melted away before the next observation becomes available then a primary goal of SCA assimilation—to correct SCA and surface albedo, preventing errors in surface energy fluxes to the atmosphere—is compromised, and, if it happens day after day (an "add/melt cycle"), soil moisture and runoff are unduly amplified. In RH04 this problem was observed at a few isolated points, but on the whole assimilation was effective, in large part because the LSM used in that study, Mosaic, suffered from over-accumulation rather than under-accumulation of snow. For an LSM such as Noah, which is prone to underestimating snow, the problem of preventing inaccurate snow melt is more critical.

The second, related difficulty in updating snow fields in an LSM is that most assimilation schemes upset the water budget without consideration for the underlying errors in the simulated precipitation and melt processes. Such introduced imbalances can compound over time and manifest themselves as soil moisture and runoff biases. As mentioned above, the advanced DA schemes capable of simultaneously updating all snow-related hydrological states at once (e.g., Clark et al. 2006) are not yet ready for global applications.

In an effort to mitigate hydrologic imbalance caused by simply adding or removing snow, we present a novel assimilation algorithm that utilizes MODIS observations from up to 72 hours ahead of simulation time. These "future" data are used to nudge the forcing air temperature and, when necessary, precipitation towards likely precursors of the observed SCA. When it is successful, this approach minimizes disruption of the local water balance and provides a smooth simulation of snow pack as informed by MODIS observations. We feel that the use of SCA observations to nudge forcing data is justified by the reliability of MODIS observations. Furthermore, the actual impact on forcing fields typically is small: snow accumulation and melt are sensitive to small changes in air temperature in the range of $0°C$, so it is rarely necessary to alter forcing air temperature by more than a few degrees C. In a coupled simulation the modification would not directly affect the atmospheric model, as air temperature within the LSM is not communicated back to the atmosphere. The modification of air temperature could indirectly affect atmospheric processes, via its influence on surface energy fluxes, but

12

that influence was found to be modest relative to the energetic impacts of snow cover itself (see Section 4). Modification of the precipitation forcing

In concept, this algorithm bears some resemblance to the EnKF update presented by Clark et al. (2006), in which snow accumulation and melt were used to update SWE indirectly on the basis of a SCA observation, and soil moisture and groundwater were updated statistically on the basis of locally-determined coefficients of variation. Beyond this the methods diverge, as our scheme employs model physics rather than statistical relationships to update hydrological fields. This avoids the need for detailed local cross-state covariance estimates, allowing for global applications.

3. Methods

(a) MODIS data

This study made use of the daily, 0.05˚-resolution MODIS climate-modeling grid-level-3 product (MOD10C1), which is based on 500-m Terra/MODIS observations (Hall et al. 2002). MOD10C1 specifies the fraction of each 0.05˚ grid cell that was observed to be snow covered, the fraction that was cloud covered, and the fraction (known as the ''confidence index'') in which the land surface was visible (i.e., not obscured by clouds, night, or other interference), at the time of the satellite overpass (approximately 10:00 A.M. local time). The MOD10C1 product has been evaluated extensively against independent satellite and ground-based datasets, and it has shown good agreement (Bitner et al. 2002; Maurer et al. 2003).

Following RH04, the reliability of a MODIS snow cover observation within a given grid square was determined using the MOD10C1 confidence index. MODIS is not cloud-penetrating, but clouds are often pervasive where snow exists, so it is essential to make prudent use of data from grid squares that are partially cloud covered, lest useful information be neglected. Taking this reasoning into account and based on a visual assessment of the credibility of the observed snow cover state at varying levels of the confidence index, it was decided that 6% is the minimum visibility for which a 0.25˚ aggregation of observations is useful. This parameter can easily be adjusted if a more appropriate value is later identified. For 0.25˚ tiles that achieved this confidence threshold, the percentage of visible, snow-covered 500-m pixels is divided by the confidence index to establish the fraction of ground-visible (cloud free) pixels that were snow covered at the time of the MODIS observation.

The relatively coarse spatial resolution of 0.25˚ was selected in order to accomplish lengthy global simulations, but MODIS would allow the application of the same algorithm at significantly higher resolution. Recently, Salomonsson and Appel (2004) have extracted fractional SCA from MODIS at 500m resolution. High resolution assimilation experiments using this product are the subject of current investigation.

(b) Assimilation procedure

The Noah LSM (version 2.7.1) was implemented for global, uncoupled simulations at 0.25˚ resolution for the periods September 2005 – June 2006 and September 2006 – June 2007. Experiments were initialized using Global Land Data Assimilation System

(GLDAS) Noah restart fields from a multi-decadal simulation parameterized and forced by a hybrid dataset (Rodell et al. 2004). Three-hourly atmospheric analyses from the Global Data Assimilation System (GDAS), the operational atmospheric DA system of NCEP (Derber et al. 1991), forced the experimental simulations. GDAS runs on a thinned Gaussian grid, with a resolution of about 0.47˚. The CPC's operational 2.5˚ 5-day Merged Analysis of Precipitation (CMAP) was used to bias-correct the higher resolution GDAS precipitation fields (Rodell et al. 2004). CMAP estimates are based on a blending of satellite data (microwave and IR) and gauge observations (Xie and Arkin 1997).

All Noah simulations were performed using the NASA Goddard Space Flight Center (GSFC) Land Information System (LIS) version 5.0. LIS is a software framework that supports the integration of observational data with coupled or uncoupled LSMs using a range of DA techniques (Kumar et al. 2006). Implementation of the assimilation algorithm within LIS allows for simulations with a number of different atmospheric forcing data sets and for application to coupled land-atmosphere modeling systems. The LIS framework also facilitates transfer of the assimilation scheme to forthcoming versions of Noah or to other, similar LSMs. In LIS-Noah, subgrid variability is captured by simulating each major land cover class within the grid cell as an independent, 1-D "tile". Gridded output is returned as the area-weighted sum of tiles within a grid cell (Rodell et al. 2004).

As discussed in Section 1, two assimilation procedures were utilized in this study, the *push* and *pull* algorithms (Figure 1). The *push* algorithm consists of a single update routine, invoked once daily for each LSM tile. It is largely analogous to the scheme used in RH04, slightly modified for Noah's snow routines.

[*push*]: At 10:00 AM local time, Noah SCA is checked against the *present* MODIS observation. At this time, if Noah differs from MODIS ($LSM_{SCA} \neq OBS_{SCA}$) then:

    a. If MODIS SCA > 0.5 and Noah SCA < 0.2, Eq. 1 is inverted in order to calculate the minimum depth of SWE that must be added to the tile to bring Noah into agreement with MODIS. This quantity is added directly to SWE. Snow depth is also updated, on the basis of added SWE and Noah's snow density routine for incoming snowfall.

    b. For MODIS SCA < 0.2 and Noah SCA > 0.5, Noah, Eq. 1 is inverted and Noah SWE is replaced with the value indicated by MODIS.

These thresholds were chosen based on the properties of the MODIS observation. The MODIS SCA product reports a "bird's eye" view of snow cover rather than an estimate of actual snow cover on the ground (as is produced by most microwave-based snow cover products). This means that in areas with tall vegetation or steep topography, MODIS frequently reports SCA below 100% even when the ground below canopy is completely snow covered. For this reason we take a conservative approach, removing snow only when MODIS SCA is particularly low (< 20%) and, in adding snow, only adding to nearly snow-free tiles for which MODIS reports considerable (>50%) snow cover. For all other tiles, we accept that $LSM_{SCA} \approx OBS_{SCA}$ and do not update the model. The *push*

algorithm differs from that of RH04 in that the volume of SWE added/removed is determined by inverting the internal Noah snow depletion curve, rather than set as a constant for the entire simulation. Use of the SDC allows for land use specificity in the assimilation update and allows us to apply the update as a continuous function of SCA. The Noah SDC is highly generalized, however, and is in no way equivalent to the detailed, geographically specific SDCs applied in watershed-scale studies (e.g., Andreadis and Lettenmaier 2006; Kolberg and Gottschalk 2006).

The *pull* algorithm comprises two update routines, the first invoked for every tile at each LSM time step, and the second invoked only once daily for each tile.

[*pull*]:

(1) At each time step, the assimilation scheme checks the simulated SCA for the tile (calculated using Eq. 1) against the most proximal *future* MODIS SCA observation. This is the same-day MODIS observation when local time is 10:00 AM or earlier and it is the next-day MODIS observation when local time is later than 10:00 AM. When the most proximal future observation is unavailable, the algorithm looks up to three days (72 hours) ahead to find a usable observation. If current Noah SCA differs from the future MODIS observation, forcing is adjusted as follows:

    a. If MODIS SCA > 0.5 and Noah SCA < 0.2, forcing air temperature is set to -3˚C for the time step. This inhibits melt and causes any incoming precipitation to be treated as snowfall.

b. If MODIS SCA < 0.2 and Noah SCA > 0.5, forcing air temperature is set to +3˚C. This promotes melt and prevents the accumulation of any new snowfall.

(2) Whenever local time is equal to 9:45AM—that is, the time step just prior to the time of MODIS observation—the precipitation field is modified directly:

a. For MODIS SCA > 0.5 and Noah SCA < 0.2, if precipitation in the forcing dataset is insufficient to produce the MODIS-observed SCA by the end of the time step, the precipitation rate is increased to the minimum rate required to produce SCA that is consistent with MODIS. Routine (1) guarantees that this added precipitation will fall as snow.

b. For MODIS SCA < 0.2 and Noah SCA > 0.5, the remaining snowpack is forcibly melted, with melt water converted to soil moisture and, if the soil saturates, to surface runoff.

All modifications to the forcing fields are recorded throughout the simulation in order to track the impact of assimilation on simulated air temperature and precipitation. Modifications to forcing imposed through assimilation are relevant only to the LSM, and not to any coupled atmospheric model; in coupled simulations, precipitation and air temperature are *inputs* to the LSM that are not reported back to the atmosphere. The modifications will, however, influence surface fluxes of energy and water. Effects on these variables are presented in Section 4.

Forcible melt of a recalcitrant snowpack (*pull* step 2b) was included in the algorithm because Noah determines the available energy for snowmelt as a function of both air

18

temperature and soil surface temperature (Koren et al. 1999).   In locations where the LSM has erroneously generated a deep snow pack, the insulating properties of the snow inhibit melt from the top. This difficulty in melting a thick snow pack from the top is inherent to the one-layer snow model in Noah 2.7.1, and would be of less concern for LSMs that contain multiple layer snow models. In practice, however, rule 2b was rarely invoked in the global 0.25˚ Noah simulations reported in this paper.

(c) Evaluation data

Model predictions of SCA and SWE were evaluated using ground-based observations wherever possible. For the United States, snow depth observations were provided by the National Weather Service Co-operative observer program (Co-op). The Co-op network does not provide direct measurements of SWE, but it is nonetheless preferable to other snow observation networks (SNOTEL, for example), both because it offers extensive coverage over the United States and because it is *not* specifically designed as a snow observation network. Observation stations designed for snow monitoring are intentionally sited in high altitude locations with deep snow accumulation, as these are the areas of greatest relevance for most snow studies. Since SCA updating is most effective in areas that have marginal snow cover or an ephemeral seasonal snow pack, Co-op stations, which are distributed randomly with respect to snow accumulation zones, are a better source of evaluation data. Snow water equivalent was estimated as 8.0% of observed depth at Co-op stations, representing an average for the dynamic range of snow density in the Noah LSM.

For locations outside of the United States, observations of snow depth were extracted from the National Climatic Data Center's Global Summary of the Day (GSOD) dataset. As with Co-op stations, GSOD observations provide information on snow presence/absence and snow depth. Unfortunately, many GSOD stations report snow observations only when snow depth is greater than zero. It is still possible to evaluate the distribution of snow cover predicted in Noah simulations against the distribution reported by GSOD stations, but with the understanding that snow-free station locations are under-represented.

4. Results

(a) SCA and SWE

Over most regions of marginal snow cover, data assimilation using the *push* or *pull* algorithm led to an increase in total snow covered area relative to open loop simulations (Figure 2). This included earlier onset of the snow season in Northern Europe and across most of North America, larger total extent of winter snow cover in the Western United States and Central Asia—but with markedly less winter snow in Tibet—and later spring melt for much of Canada and, with the exception of Tibet, Eurasia.

Comparisons with *in situ* reports of snow presence/absence indicate that DA-informed simulations of snow cover were substantially more accurate than the open loop simulation. For reporting Co-op stations in the contiguous United States, open loop simulations with Noah systematically under-estimated snow presence (Figure 3). The assimilation of MODIS SCA observations corrected this bias, bringing the model into

better agreement with observations: for the winter of 2005-6 (Dec-Feb), 32% of all daily

Co-op snow reports indicated that snow was present. The open loop simulation had non-

zero snow at only 19% of the corresponding day-locations, while in the DA assimilations

the average was 23% for *push* and 30% for *pull*. Results were similar for the winter of

2006-7: 40% for Co-op stations, 25% for open loop simulations, and 29% and 38% for

push and *pull*, respectively. Data for regions outside of the United States are less

complete, but they show a similar pattern. In high latitude regions like Central Canada

and Siberia, the positive impact of DA came primarily at the beginning and/or end of the

snow season (Figure 3), while in mid-latitude regions with incomplete snow cover,

improvements were seen throughout the winter (e.g., Mongolia, Figure 3). In all cases,

pull had a larger influence on Noah simulations than *push*, drawing the simulation into

better agreement with available station data. Unfortunately, station reports from Tibet

were too limited to allow for a full station-based evaluation of DA results in this

interesting region. However, the general tendency of DA to produce patchy, rather than

complete, snow cover for Tibet is consistent with the known character of snow cover on

the Tibetan plateau, as established in field survey and independent remote sensing

analyses (Qin et al. 2006). MODIS SCA observations, for their part, have been validated

for Tibet in a focused, regional-scale study (Pu et al. 2007), further increasing our

confidence in DA results for the plateau.

With respect to snow volume, DA had a positive influence on the simulation of SWE in

regions with partial or transient snow cover, including the U.S. Southwest, where snow

accumulation is significant only in elevated areas and shows strong inter-annual

variability, the U.S. High Plains, and the Mongolian Steppe (Figure 4).   Following the

pattern observed for SCA, DA tended to increase SWE relative to open loop simulations

in most regions. In regions with deep seasonal snowpack, assimilation was only able to

provide a marginal improvement in the simulation of SWE. Such was the case for the

United States "West Coast" focus region, which included the Sierra Nevada and Cascade

ranges. DA increased SCA in these ranges (see Figure 2), but was not able to improve

model simulation of SWE significantly (Figure 4), because MODIS provides no

information on snow mass or depth.

(b) Hydrological fluxes

As the SCA and SWE results indicate, the *pull* approach applied MODIS information

more effectively than the *push* approach, primarily because it offset discrepancies

between the satellite observation and atmospheric forcing data. By nudging the

atmospheric forcing into consistency with the MODIS observation, the algorithm updated

snow fields in a more robust manner, reducing the incidence of daily add/melt cycles and

related artifacts. Thus *pull* maintained a local hydrological balance at all points

throughout the simulation. In contrast, the simple addition or removal of snow in the

push simulation overwhelmed the water balance in certain locations.

Figure 5 shows an example of this for a location in California where MODIS observed

partial snow cover throughout the winter months, while open loop Noah simulations

failed to capture any significant snow accumulation (Figure 5A). Both the *push* and *pull*

integrations effectively corrected the low snow bias, adding SWE to the simulation

(Figure 5B). *Push*, however, accomplished this by the direct addition (removal) of snow to (from) the land surface, which caused non-physical imbalances in the local water balance (Figure 5C). *Pull* maintained the local hydrological balance as effectively as open loop simulations by anticipating the presence of snow and reducing air temperature (Figure 5G). The relatively modest reduction in air temperature was sufficient to change the phase of incoming precipitation to snow (Figure 5E) from rain (Figure 5F). The physically consistent approach to snow updates also had an influence on snow melt (Figure 5H) and, by extension, runoff (Figure 5D) and soil moisture.

Figure 6 demonstrates the advantages of *pull* for a location where DA had to remove snow from the model. This was not nearly as common in the Noah simulations as it was in the RH04 Mosaic simulations, but it was necessary in some regions of Siberia where the onset of the snow season was premature in the open loop (see Figure 2). At this particular location, MODIS observed a sporadic onset for the snow season, as snow cover was variable during the month of October (Figure 6A). Air temperature hovered around freezing (Figure 6G), making the model prone to error in snowfall and melt processes. Both *push* and *pull* captured observed variability in snow cover, including a reduction in snow cover in the middle of the month (Figure 6B), but *push* did so by simply removing snow from the model, causing a hydrological imbalance (Figure 6C). *Pull* maintained the local water balance. Snow was removed by slightly raising air temperature (Figure 6G), leading to snow melt (Figure 6H).

The secondary *pull* add-snow procedure—increasing the local precipitation rate when air temperature modifications failed to produce an adequate snow cover—preserves the surface water balance at the expense of a possible precipitation bias. That consequence should be examined closely in any application. For the simulations performed in this study, the influence of *pull* on precipitation was substantial in some locations, but differences between *pull* and open loop precipitation were generally within the uncertainty level, i.e., the range of estimates from various global precipitation datasets. In fact, the *pull* algorithm often brought the open loop precipitation (disaggregated CMAP) into better agreement with alternative forcing datasets (Table 1). One exception is for high latitude regions in the spring. In these regions, the DA-induced addition of precipitation due to the *pull* algorithm did sometimes impose a wet bias beyond the range of common precipitation datasets. This assimilation artifact reflects a limitation in the MODIS SCA data. Because MODIS depends on visible and near infrared data to determine snow cover, the sensor cannot provide SCA estimates at high latitudes during winter. During this extended data gap, the model has the opportunity to drift to lower SCA values (e.g., Figure 3, Central Canada). When the MODIS record for these regions resumes in spring, a relatively large volume of snow must be added to the simulation in order to regain accurate snow cover. To address this issue, we have begun to investigate the use of multisensor snow cover products (Helfrich et al. 2007; Romanov et al. 2003) that utilize high resolution visible/near-infrared observations whenever available but use microwave data to fill in data gaps at high latitudes. It is anticipated that such multisensor products will correct for any artificial wet bias that *pull* produces at high latitudes.

Pull generally produced more realistic snow melt, soil moisture, and runoff than *push*. This was most obvious in locations where *push* repeatedly caused add/melt cycles over the course of the snow season (e.g., Figure 7). These cycles resulted from inconsistencies between observation (SCA > 0.5) and atmospheric forcing (T_{air} > 0˚C). By making small adjustments to air temperature (Figure 7G), *pull* made it possible for the LSM to retain an applied positive snow increment, rather than melt it away (Figure 7B,C,H). Even under less dramatic circumstances, differences between *pull* and *push* can accumulate over the season to have a substantial impact on total snow melt, as well as the associated fields of soil moisture and runoff.

 (c) Energy fluxes

As expected, data assimilation had a substantial impact on the surface energy balance and on land-atmosphere energy fluxes. Changes to SCA altered surface albedo, which in turn influenced radiative and turbulent fluxes. These effects were most pronounced at mid-latitudes during winter and at high latitudes in fall and spring, and were quite substantial for some regions. In the US West, for example, DA increased snow covered area and albedo, causing a reduction in net radiation and sensible heat flux in winter (Table 2). The effects of the SCA update persisted into spring, when snow melt in the DA simulations led to increased soil moisture, enhanced latent heat flux, and slightly reduced surface temperature. Despite more widespread snow cover in the *pull* simulation, soil moisture and latent heat flux were somewhat greater in the *push* simulation because of the add/melt cycles in the US West. The influence of DA on energy fluxes was also

25

observed in mid-latitude Eurasia. In Mongolia, DA produced simulations with increased wintertime SCA and albedo and substantially decreased net radiation and sensible heat flux. The persistence of snow memory in the form of soil moisture was smaller in this region than it was in the US West.

At high latitudes where winter snow cover was not ephemeral, DA had minimal impact on energy fluxes during winter, but it had substantial impacts in spring (Table 2: Central Canada and Siberia). Both *push* and *pull* increased springtime snow cover and surface albedo in these regions, which in turn reduced net shortwave radiation at the surface. Outgoing longwave radiation also decreased, owing to reduced surface temperature. The reduction in surface temperature was caused by increased snow cover and, in the case of the *pull* simulation, reduced air temperature. Sensible heat flux diminished relative to open loop due to the combined effects of reduced net surface radiation and enhanced latent heat flux.

These results demonstrate the value of SCA observations for coupled land-atmosphere simulations. They also allay a concern associated with the *pull* algorithm: that manipulation of air temperature might lead to unrealistic radiation and energy fluxes. For example, in locations where the *pull* algorithm reduces air temperature in order to increase SCA, it is possible that the enhanced surface-to-air temperature gradient might lead to increased surface sensible heat flux even though the addition of snow would be expected to reduce it. In this application, it was found that *pull* imposed only small changes in the air temperature forcing field, and any influence that this had on turbulent

26

fluxes was small relative to the influence of improving the model's representation of SCA. This is clear from the fact that *push* and *pull* had similar influences on energy fluxes in all regions: increased SCA led to substantial reductions in sensible heat flux, and any mitigation of this due to enhanced surface to air temperature gradient in *pull* was negligible both in the monthly average (as shown in Table 2) and on daily and 3-hourly timescales. Similarly, the influence of DA on radiative fluxes was dominated by the impact of SCA on surface properties rather than the influence of *pull* on atmospheric forcing fields. Even in high latitude regions such as Central Canada, where *pull* reduced surface temperatures and net longwave radiation relative to *push*, the energetic differences between simulations is attributed to the fact that *pull* more effectively maintained snow cover, leading to larger values of SCA. The direct manipulation of air temperature (Table 1) was small relative to simulated differences in surface temperature (Table 2), and would be expected to have the opposite influence on longwave radiation than was observed in the simulation: the magnitude of net outgoing longwave radiation at the surface was reduced in *pull* relative to other simulations, even though the manipulation of air temperature decreased incoming radiation, which would, on its own, have increased outgoing net radiation.

5. Discussion

The assimilation of MODIS SCA observations to the Noah LSM yielded improved estimates of snow cover in offline global simulations. This had a substantial impact on the surface radiation balance, indicating that the technique would be of value in coupled land-atmosphere simulations. Regions where assimilation had a large impact include the

27

western United States and Mongolia, in winter, and Siberia and Central Canada in spring. Both assimilation schemes tested in this paper—the rule-based *push* assimilation scheme and the *pull* assimilation scheme that updated air temperature and precipitation fields— improved the simulation of SCA and SWE relative to open loop simulations. *Pull* tended to produce more robust results, in large part because positive snow increments in *push* often melted away rapidly. Any unintended influence that *pull* might have had on surface energy fluxes as a byproduct of air temperature manipulations was small compared to the effect of updating SCA. Improved realism in the simulation of SCA and associated surface energy fluxes is important for retrospective climate analyses and, in the context of coupled models, for seasonal forecasts. This is particularly true for regions like Siberia, where variability in SCA is known to have a significant impact on atmospheric circulations and climate throughout the northern hemisphere (Gong et al. 2003), and for mid-latitude regions such as the United States Great Plains, where snow influences springtime soil moisture and vegetation, both of which are involved in important land-atmosphere feedbacks on climate (Koster et al. 2004). The degree to which local improvements in the simulation of SCA lead to improved seasonal predictions on the regional scale will, of course, depend on the accuracy of model physics and parameterizations (Schlosser and Mocko 2003).

With respect to hydrological variables, the benefits of data assimilation were more modest. The assimilation of SCA is inherently limited in this regard, as most snow is stored in regions of deep snow, where SCA observations have little information to provide beyond the first few weeks and last few weeks of the snow season. In evaluation

against snow depth measurements from available surface stations, data assimilation did appear to improve simulation of SWE in some regions. Not surprisingly, these were regions of ephemeral snow cover, where SCA observations are most indicative of SWE. The *pull* algorithm caused a significant increase in precipitation, however, the CMAP-based forcing data used in the experiments had a low bias compared with other precipitation products, and the resulting total precipitation in the *pull* simulation was somewhere between CMAP and the others. Consequently, *pull* also tended to generate more runoff, latent heat flux, and soil moisture than open loop. *Push*, in contrast, had mixed hydrological effects, as the net impact of add/melt and remove/accumulate cycles somewhat offset each other when averaged across focus regions. These results could not be evaluated reliably against observations, owing to the many possible sources of biases in modeled runoff and soil moisture, and hence the difficulty determining an improvement or degradation.

In high latitude regions the hydrological benefits of data assimilation were limited by the fact that MODIS cannot observe surface conditions without daylight or during periods of extended cloud cover. This problem will be mitigated by the use of multisensor snow cover products in future studies. Nonetheless, MODIS observations alone do provide significant information for many snow-covered regions of the world.

In summary, the shortcomings of existing snow cover assimilation schemes motivated the development of the new *pull* algorithm. In particular, the algorithm overcomes a key limitation: in cases where the atmospheric forcing fields contradict the assimilated

observation, updates to SWE can be quickly nullified by subsequent snow melt or (less frequently) accumulation. The new scheme compels the air temperature and precipitation to complement the near future SCA observation, thus preserving the update. In our experimental simulation, this led to simulated SCA values that were higher than *push* and the open loop, and that were more consistent with ground based observations. The second shortcoming we addressed was the tendency of assimilation schemes to disrupt the local water balance. *Pull* inherently prevents hydrological imbalance and limits the add/melt and remove/accumulate cycles that produce undesirable artifacts in the simulated snow melt, soil moisture, and runoff fields. Nevertheless, there is still room for improvement in the use of data assimilation to improve simulations of snow hydrology on the global scale. More reliable satellite retrievals of SWE are needed to update snow fields in areas of 100% cover. In the interim, the application of multisensor SCA products will fill gaps in the MODIS product, allowing for smoother and more complete updates in high latitude and cloud covered regions.

References

Anderson, E. A., 1973: National weather service river forecast system--snow accumulation and ablation model. NOAA Technical Memorandum NWS HYDRO-17.

Andreadis, K. M. and D. P. Lettenmaier, 2006: Assimilating remotely sensed snow observations into a macroscale hydrology model. *Advances in Water Resources*, **29,** 872-886.

Baker, D. G., D. L. Ruschy, R. H. Skaggs, and D. B. Wall, 1992: Air-Temperature and Radiation Depressions Associated with a Snow Cover. *Journal of Applied Meteorology*, **31,** 247-254.

Bamzai, A. S. and J. Shukla, 1999: Relation between Eurasian snow cover, snow depth, and the Indian summer monsoon: An observational study. *Journal of Climate*, **12,** 3117-3132.

Bitner, D., T. Carroll, D. Cline, and P. Romanov, 2002: An assessment of the differences between three satellite snow cover mapping techniques. *Hydrological Processes*, **16,** 3723-3733.

Brubaker, K. L., R. T. Pinker, and E. Deviatova, 2005: Evaluation and comparison of MODIS and IMS snow-cover estimates for the continental United States using station data. *Journal of Hydrometeorology*, **6,** 1002-1017.

Chang, A. T. C., J. L. Foster, and D. K. Hall, 1987: Nimbus-7 SMMR derived global snow cover parameters. *Ann. Glaciol.*, **9,** 39-44.

Chang, A. T. C., J. L. Foster, D. K. Hall, H. W. Powell, and Y. L. Chien, 1990: *Nimbus-7 SMMR derived global snow cover and snow depth data set. The Pilot Land Data System*, NASA Goddard Space Flight Center, 40 pp.

Chang, A. T. C., R. E. J. Kelly, E. G. Josberger, R. L. Armstrong, J. L. Foster, and N. M. Mognard, 2005: Analysis of ground-measured and passive-microwave-derived snow depth variations in midwinter across the northern Great Plains. *Journal of Hydrometeorology*, **6,** 20-33.

Chen, F., K. Mitchell, J. Schaake, Y. K. Xue, H. L. Pan, V. Koren, Q. Y. Duan, M. Ek, and A. Betts, 1996: Modeling of land surface evaporation by four schemes and comparison with FIFE observations. *Journal of Geophysical Research-Atmospheres*, **101,** 7251-7268.

Clark, M. P., A. G. Slater, A. P. Barrett, L. E. Hay, G. J. McCabe, B. Rajagopalan, and G. H. Leavesley, 2006: Assimilation of snow covered area information into hydrologic and land-surface models. *Advances in Water Resources*, **29,** 1209-1221.

Cohen, J. and D. Entekhabi, 2001: The influence of snow cover on Northern Hemisphere climate variability. *Atmosphere-Ocean*, **39,** 35-53.

Cordisco, E., C. Prigent, and F. Aires, 2006: Snow characterization at a global scale with passive microwave satellite observations. *Journal of Geophysical Research-Atmospheres*, **111**.

Decker, K. L. M., D. Wang, C. Waite, and T. Scherbatskoy, 2003: Snow removal and ambient air temperature effects on forest soil temperatures in Northern Vermont. *Soil Science Society of America Journal*, **67,** 1234-1242.

Derber, J. C., D. F. Parrish, and S. J. Lord, 1991: The new global operational analysis system at the National Meteorological Center. *Weather Forecasting*, **6,** 538-547.

Dery, S. J., J. Sheffield, and E. F. Wood, 2005: Connectivity between Eurasian snow cover extent and Canadian snow water equivalent and river discharge. *Journal of Geophysical Research-Atmospheres*, **110**.

Durand, M. and S. A. Margulis, 2006: Feasibility test of multifrequency radiometric data assimilation to estimate snow water equivalent. *Journal of Hydrometeorology*, **7,** 443-457.

Ek, M. B., K. E. Mitchell, Y. Lin, E. Rogers, P. Grunmann, V. Koren, G. Gayno, and J. D. Tarpley, 2003: Implementation of Noah land surface model advances in the National Centers for Environmental Prediction operational mesoscale Eta model. *Journal of Geophysical Research-Atmospheres*, **108**.

Elguindi, N., B. Hanson, and D. Leathers, 2005: The effects of snow cover on midlatitude cyclones in the great plains. *Journal of Hydrometeorology*, **6,** 263-279.

Ellis, A. W. and D. J. Leathers, 1999: Analysis of cold airmass temperature modification across the US Great Plains as a consequence of snow depth and albedo. *Journal of Applied Meteorology*, **38,** 696-711.

Flerchinger, G. N., K. R. Cooley, and Y. Deng, 1994: Impacts of Spatially and Temporally Varying Snowmelt on Subsurface Flow in a Mountainous Watershed .1. Snowmelt Simulation. *Hydrological Sciences Journal-Journal Des Sciences Hydrologiques*, **39,** 507-520.

Foster, J., G. Liston, R. Koster, R. Essery, H. Behr, L. Dumenil, D. Verseghy, S. Thompson, D. Pollard, and J. Cohen, 1996: Snow cover and snow mass intercomparisons of general circulation models and remotely sensed datasets. *Journal of Climate*, **9,** 409-426.

Gong, G., D. Entekhabi, and J. Cohen, 2003: Modeled Northern Hemisphere winter climate response to realistic Siberian snow anomalies. *Journal of Climate*, **16,** 3917-3931.

Gong, G., J. Cohen, D. Entekhabi, and Y. Ge, 2007: Hemispheric-scale climate response to Northern Eurasia land surface characteristics and snow anomalies. *Global and Planetary Change*, **56,** 359-370.

Hall, D. K., 1988: Assessment of polar climate change using satellite technology. *Rev. Geophys.*, **26,** 26-39.

Hall, D. K., G. A. Riggs, V. V. Salomonson, N. E. DiGirolamo, and K. J. Bayr, 2002: MODIS snow-cover products. *Remote Sensing of Environment*, **83,** 181-194.

Helfrich, S. R., D. McNamara, B. H. Ramsay, T. Baldwin, and T. Kasheta, 2007: Enhancements to, and forthcoming developments in the Interactive Multisensor Snow and Ice Mapping System (IMS). *Hydrological Processes*, **21,** 1576-1586.

Huffman, G. J., R. F. Adler, D. T. Bolvin, G. J. Gu, E. J. Nelkin, K. P. Bowman, Y. Hong, E. F. Stocker, and D. B. Wolff, 2007: The TRMM multisatellite precipitation analysis (TMPA): Quasi-global, multiyear, combined-sensor precipitation estimates at fine scales. *Journal of Hydrometeorology*, **8,** 38-55.

Kolberg, S., H. Rue, and L. Gottschalk, 2006: A Bayesian spatial assimilation scheme for snow coverage observations in a gridded snow model. *Hydrology and Earth System Sciences*, **10,** 369-381.

Kolberg, S. A. and L. Gottschalk, 2006: Updating of snow depletion curve with remote sensing data. *Hydrological Processes*, **20,** 2363-2380.

Koren, V., J. Schaake, K. Mitchell, Q. Y. Duan, F. Chen, and J. M. Baker, 1999: A parameterization of snowpack and frozen ground intended for NCEP weather and climate models. *Journal of Geophysical Research-Atmospheres*, **104,** 19569-19585.

Koster, R. D., P. A. Dirmeyer, Z. C. Guo, G. Bonan, E. Chan, P. Cox, C. T. Gordon, S. Kanae, E. Kowalczyk, D. Lawrence, P. Liu, C. H. Lu, S. Malyshev, B. McAvaney, K. Mitchell, D. Mocko, T. Oki, K. Oleson, A. Pitman, Y. C. Sud, C. M. Taylor, D. Verseghy, R. Vasic, Y. K. Xue, and T. Yamada, 2004: Regions of strong coupling between soil moisture and precipitation. *Science*, **305,** 1138-1140.

Kumar, S. V., C. D. Peters-Lidard, Y. Tian, P. R. Houser, J. Geiger, S. Olden, L. Lighty, J. L. Eastman, B. Doty, P. Dirmeyer, J. Adams, K. Mitchell, E. F. Wood, and J. Sheffield, 2006: Land information system: An interoperable framework for high resolution land surface modeling. *Environmental Modelling & Software*, **21,** 1402-1415.

Liston, G. E., 2004: Representing subgrid snow cover heterogeneities in regional and global models. *Journal of Climate*, **17,** 1381-1397.

Marsh, P., 1999: Snowcover formation and melt: recent advances and future prospects. *Hydrological Processes*, **13,** 2117-2134.

Maurer, E. P., J. D. Rhoads, R. O. Dubayah, and D. P. Lettenmaier, 2003: Evaluation of the snow-covered area data product from MODIS. *Hydrological Processes*, **17,** 59-71.

Pitman, A. J., 2003: The evolution of, and revolution in, land surface schemes designed for climate models. *International Journal of Climatology*, **23,** 479-510.

Pu, Z. X., L. Xu, and V. V. Salomonson, 2007: MODIS/Terra observed seasonal variations of snow cover over the Tibetan Plateau. *Geophysical Research Letters*, **34**.

Qin, D. H., S. Y. Liu, and P. J. Li, 2006: Snow cover distribution, variability, and response to climate change in western China. *Journal of Climate*, **19,** 1820-1833.

Ren, J., H. Y. Liu, Y. Yin, and S. Y. He, 2007: Drivers of greening trend across vertically distributed biomes in temperate arid Asia. *Geophysical Research Letters*, **34**.

Rodell, M. and P. R. Houser, 2004: Updating a land surface model with MODIS-derived snow cover. *Journal of Hydrometeorology*, **5,** 1064-1075.

Rodell, M., P. R. Houser, U. Jambor, J. Gottschalck, K. Mitchell, C. J. Meng, K. Arsenault, B. Cosgrove, J. Radakovich, M. Bosilovich, J. K. Entin, J. P. Walker, D. Lohmann, and D. Toll, 2004: The global land data assimilation system. *Bulletin of the American Meteorological Society*, **85,** 381-+.

Roesch, A., M. Wild, H. Gilgen, and A. Ohmura, 2001: A new snow cover fraction parametrization for the ECHAM4 GCM. *Climate Dynamics*, **17,** 933-946.

Romanov, P., D. Tarpley, G. Gutman, and T. Carroll, 2003: Mapping and monitoring of the snow cover fraction over North America. *Journal of Geophysical Research-Atmospheres*, **108**.

Salomonson, V. V. and I. Appel, 2004: Estimating fractional snow cover from MODIS using the normalized difference snow index. *Remote Sensing of Environment*, **89,** 351-360.

Schlosser, C. A. and D. M. Mocko, 2003: Impact of snow conditions in spring dynamical seasonal predictions. *Journal of Geophysical Research-Atmospheres*, **108**.

Stieglitz, M., A. Ducharne, R. D. Koster, and M. J. Suarez, 2001: The impact of detailed snow physics on the simulation of snowcover and subsurface thermodynamics at continental scales. *Journal of Hydrometeorology*, **2,** 228-242.

Takata, K., S. Emori, and T. Watanabe, 2003: Development of the minimal advanced treatments of surface interaction and runoff. *Global and Planetary Change*, **38,** 209-222.

Xie, P. P. and P. A. Arkin, 1997: Global precipitation: A 17-year monthly analysis based on gauge observations, satellite estimates, and numerical model outputs. *Bulletin of the American Meteorological Society*, **78,** 2539-2558.

Zaitchik, B. F., J. P. Evans, and R. B. Smith, 2007: Regional impact of an elevated heat source: the Zagros plateau of Iran. *Journal of Hydrometeorology*, **20,** 4133-4146.

Tables

Table 1: Precipitation and air temperature during the 2006-7 snow season (September 2006 – May 2007) as reported by GDAS, CMAP, the NCEP-NCAR Reanalysis Project v2 and the TRMM 3B43 merged precipitation product (Huffman et al. 2007) not available for high latitude regions), and as estimated in the *Pull* assimilation integration. Data are shown for two regions in North America and two in Eurasia, as mapped on Figure 2. All simulations in this paper used GDAS atmospheric forcing corrected with CMAP precipitation. Thus, the combination of GDAS air temperature with CMAP precipitation is representative of forcing fields in the Open Loop and *Push* integrations. The *Pull* fields of precipitation and air temperature represent the effects of the assimilation algorithm on a background of GDAS/CMAP forcing.

		USWest					C. Canada				
		GDAS	CMAP	NNRP	TRMM	*Pull*	GDAS	CMAP	NNRP	TRMM	*Pull*
Precip (mm/day)	Oct	1.39	0.78	1.19	1.02	0.92	2.01	1.66	2.39	--	1.90
	Jan	0.73	0.33	1.07	1.14	0.58	0.87	0.59	0.79	--	0.60
	Apr	1.81	0.85	1.55	1.06	1.14	1.33	0.66	1.22	--	1.66
	Total	12.02	6.83	11.56	9.75	8.87	13.53	9.86	13.90	--	11.46
Tair (K)	Oct	280.7	--	280.9	--	280.2	274.1	--	272.8	--	273.5
	Jan	267.6	--	267.0	--	267.7	257.4	--	255.2	--	257.5
	Apr	280.0	--	279.2	--	279.4	271.2	--	268.0	--	270.1
	Average	277.5	--	277.2	--	277.2	267.7	--	265.9	--	267.3

		Mongolia					Siberia				
		GDAS	CMAP	NNRP	TRMM	*Pull*	GDAS	CMAP	NNRP	TRMM	*Pull*
Precip (mm/day)	Oct	0.25	0.22	0.23	0.28	0.31	1.42	0.99	1.31	--	1.29
	Jan	0.10	0.05	0.21	0.08	0.16	0.70	0.52	0.69	--	0.58
	Apr	0.38	0.25	0.57	0.29	0.35	1.33	0.48	2.42	--	1.94
	Total	2.41	1.86	2.85	2.27	2.71	11.76	7.22	10.69	--	10.09
Tair (K)	Oct	279.1	--	276.6	--	279.0	266.6	--	264.6	--	268.0
	Jan	257.6	--	254.9	--	259.2	254.3	--	253.4	--	254.9
	Apr	279.0	--	276.9	--	278.8	270.2	--	286.2	--	269.6
	Average	272.3	--	270.2	--	272.9	262.3	--	261.1	--	262.7

Table 2: Snow, hydrology, and surface energy variables for the open loop, *push*, and *pull* simulations for October, January, and April of the 2006-7 snow season. All values are monthly averages. Gray shading indicates values that are referenced in the text. SW = shortwave radiation, LW = longwave radiation, R_{net} = net surface radation, H = sensible heat flux, λE = latent heat flux, SM = soil moisture, Q = total runoff.

		USWest			C. Canada			Mongolia			Siberia		
		open	push	pull	open	push	pull	open	push	pull	open	push	pull
SCA	Oct	0.01	0.02	0.04	0.16	0.21	0.30	0.01	0.03	0.04	0.38	0.38	0.42
	Jan	0.27	0.36	0.53	0.99	0.98	0.99	0.33	0.42	0.52	0.98	0.97	0.98
	Apr	0.02	0.03	0.05	0.38	0.43	0.58	0.02	0.02	0.03	0.40	0.46	0.63
Albedo	Oct	0.20	0.21	0.21	0.21	0.23	0.25	0.24	0.25	0.26	0.27	0.27	0.28
	Jan	0.29	0.32	0.38	0.46	0.46	0.46	0.39	0.43	0.48	0.42	0.41	0.42
	Apr	0.19	0.19	0.20	0.28	0.29	0.33	0.23	0.23	0.23	0.26	0.28	0.32
Net SW (Wm^{-2})	Oct	126.4	125.7	125.1	63.9	62.8	61.4	121.9	120.6	119.7	59.6	58.9	57.9
	Jan	79.5	74.7	67.9	21.4	21.5	21.3	55.1	50.9	46.8	13.4	13.5	13.4
	Apr	194.8	193.5	192.2	138.7	135.5	128.6	207.5	207.3	206.3	141.0	137.3	128.8
Net LW (Wm^{-2})	Oct	-87.3	-87.0	-84.4	-55.9	-55.4	-51.7	-97.2	-96.9	-96.0	-61.3	-60.6	-64.5
	Jan	-72.0	-70.9	-70.2	-44.8	-43.1	-44.8	-70.7	-69.8	-74.6	-45.0	-44.6	-46.7
	Apr	-91.9	-90.9	-87.2	-59.6	-58.0	-51.9	-108.0	-107.9	-106.7	-62.6	-61.3	-57.2
R_{net} (Wm^{-2})	Oct	39.1	38.7	40.7	8.0	7.4	9.7	24.7	23.7	23.7	-1.7	-1.8	-6.6
	Jan	7.4	3.8	-2.3	-23.4	-21.6	-23.4	-15.6	-18.9	-27.8	-31.7	-31.1	-33.3
	Apr	102.9	102.6	105.0	79.1	77.5	76.7	99.6	99.4	99.6	78.4	76.0	71.6
$T_{surface}$ (K)	Oct	281.4	281.4	280.8	274.1	274.0	273.2	278.6	278.5	278.3	266.4	266.2	267.1
	Jan	267.3	267.1	266.9	256.6	256.1	256.5	255.7	255.5	256.6	252.2	252.1	252.7
	Apr	282.2	282.0	281.4	272.6	272.2	271.0	280.2	280.2	280.0	271.8	271.5	270.6
H (Wm^{-2})	Oct	34.0	32.7	35.8	7.8	6.1	10.3	26.3	24.6	25.2	7.2	6.2	0.6
	Jan	13.3	8.8	5.2	-4.5	-8.4	-4.8	-6.2	-8.6	-14.2	-16.5	-17.3	-17.7
	Apr	71.1	64.6	68.1	46.3	38.5	40.3	79.9	78.1	74.4	49.8	41.2	35.6
λE (Wm^{-2})	Oct	11.8	12.7	11.9	11.4	12.4	11.5	4.9	5.7	5.4	7.8	8.2	8.9
	Jan	3.3	5.3	5.3	2.4	1.7	2.5	0.6	0.7	-0.2	-0.6	-0.7	-0.6
	Apr	25.0	30.1	28.8	20.9	27.2	26.5	8.1	9.5	12.6	15.0	21.5	22.8
SWE (mm)	Oct	0.08	0.22	0.43	2.89	3.62	6.17	0.11	0.27	0.48	6.36	6.63	8.26
	Jan	4.52	5.14	9.37	58.08	58.16	66.08	3.33	4.69	6.73	72.03	68.24	71.40
	Apr	0.18	0.35	0.65	24.75	24.63	31.63	0.29	0.24	0.41	24.46	22.53	27.78
SM (m/m)	Oct	0.22	0.22	0.22	0.39	0.40	0.39	0.18	0.18	0.18	0.31	0.32	0.32
	Jan	0.26	0.28	0.28	0.42	0.43	0.42	0.18	0.18	0.19	0.31	0.32	0.33
	Apr	0.28	0.32	0.33	0.46	0.51	0.47	0.18	0.18	0.21	0.36	0.39	0.40
Q (mm/day)	Oct	0.01	0.01	0.01	0.14	0.15	0.13	0.00	0.00	0.00	0.05	0.06	0.12
	Jan	0.05	0.07	0.09	0.05	0.05	0.07	0.00	0.00	0.01	0.00	0.00	0.09
	Apr	0.05	0.10	0.14	0.85	0.69	1.38	0.01	0.01	0.02	0.80	0.89	1.21

Figures

Figure 1: General format of the two MODIS SCA assimilation algorithms used in the study. (A) A rule-based direct insertion algorithm ("Push"), in which observed SCA is used to update model SWE by inverting the snow depletion curve within the model to obtain an effective "Observed SWE" consistent with model parameters. (B) a forcing modification algorithm ("Pull") in which information from a future MODIS observation is used to nudge snow accumulation and melt processes within the model. This is accomplished by adjusting air temperature or, when that fails, ground temperature and precipitation.
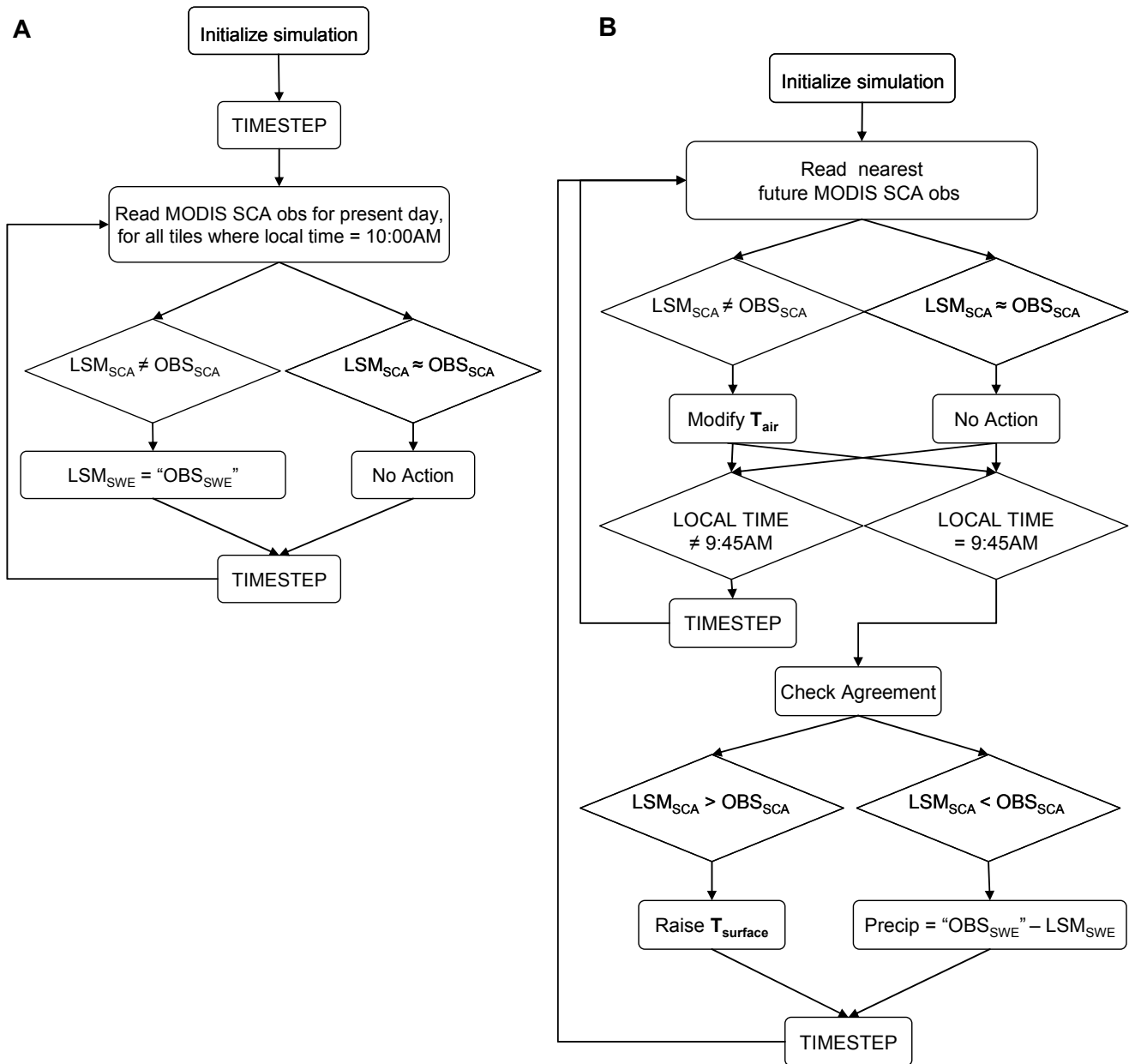
Figure 2: Monthly averaged snow covered area in the *Pull* simulation (top panel), the open loop simulation (middle panel), and the difference between the two (Pull – open loop; bottom panel), for three months during the 2006-7 snow season. Red boxes indicate the locations of the United States West, Mongolia, Central Canada, and Siberia focus regions.
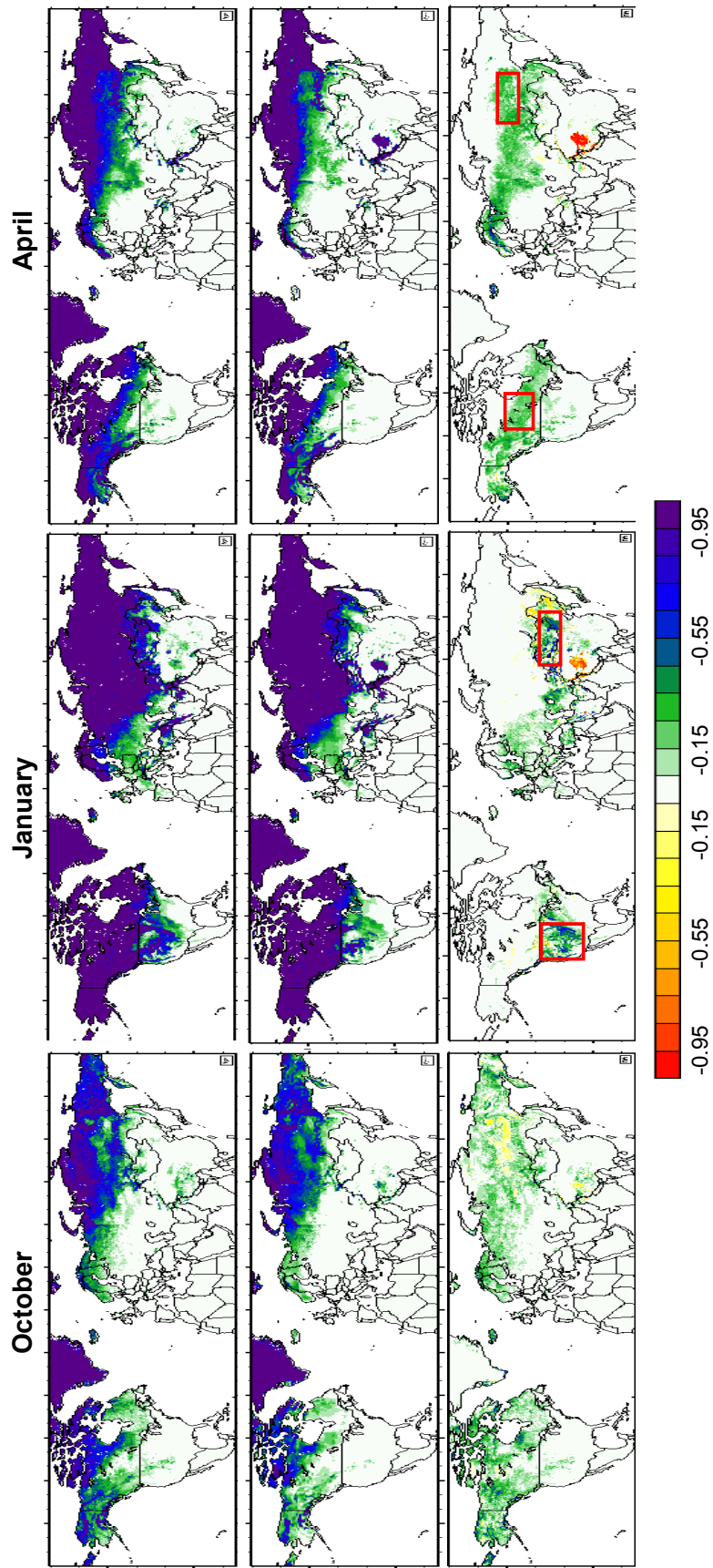
Figure 3: Percent of stations reporting snow cover for Co-op sites in the contiguous US and GSOD sites in Central Canada, Mongolia, and Siberia, along with the percentage of those site locations that had snow cover in open loop, *push* and *pull* simulations.
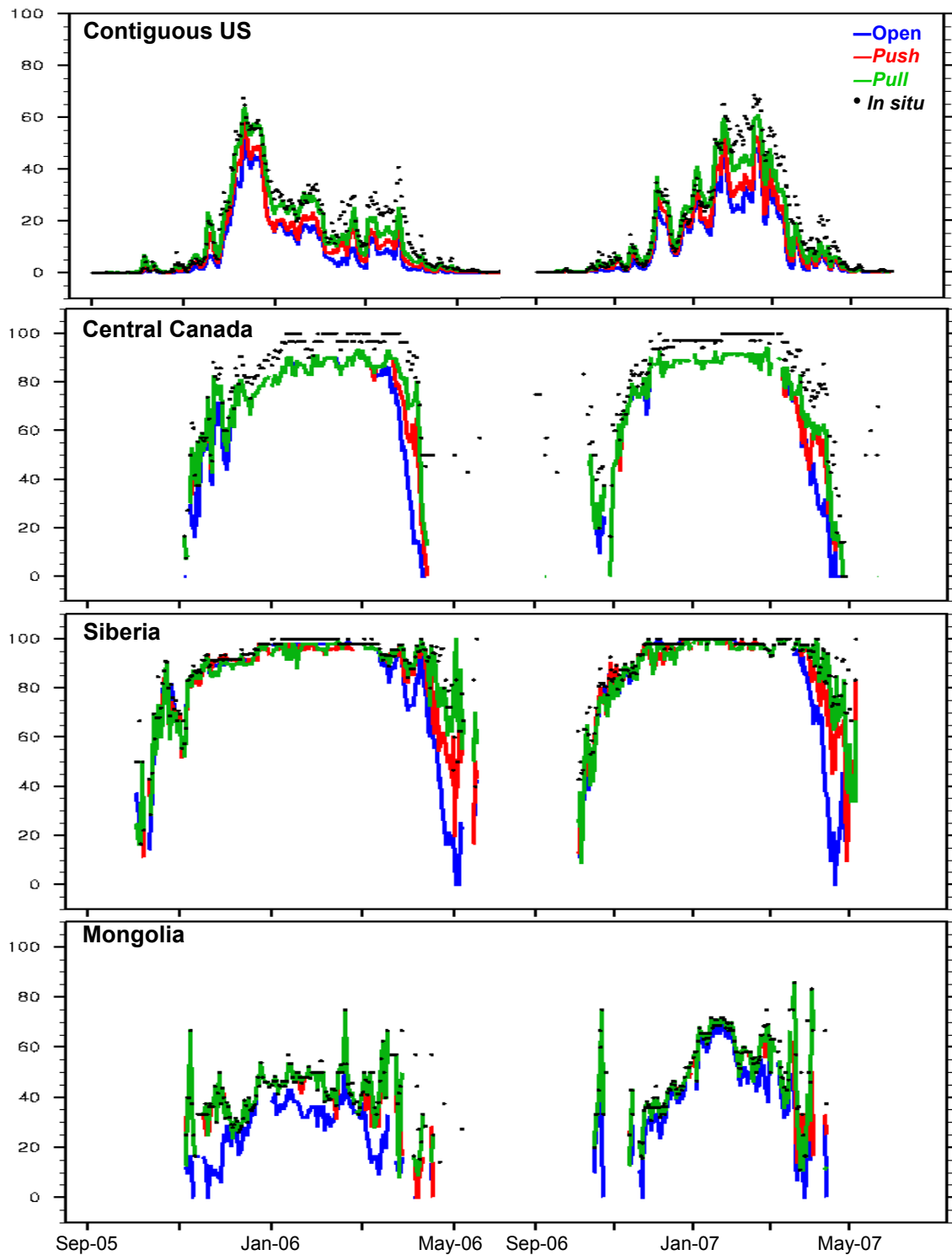
Figure 4: Snow water equivalent, as predicted in Noah simulations and as estimated from snow depth reports at the locations of Co-op and (for Mongolia) GSOD observing stations. Maps within each panel indicate the averaging region within the United States. The Mongolia averaging region is the same as that mapped in Figure 2. N = number of stations used to calculate the average.
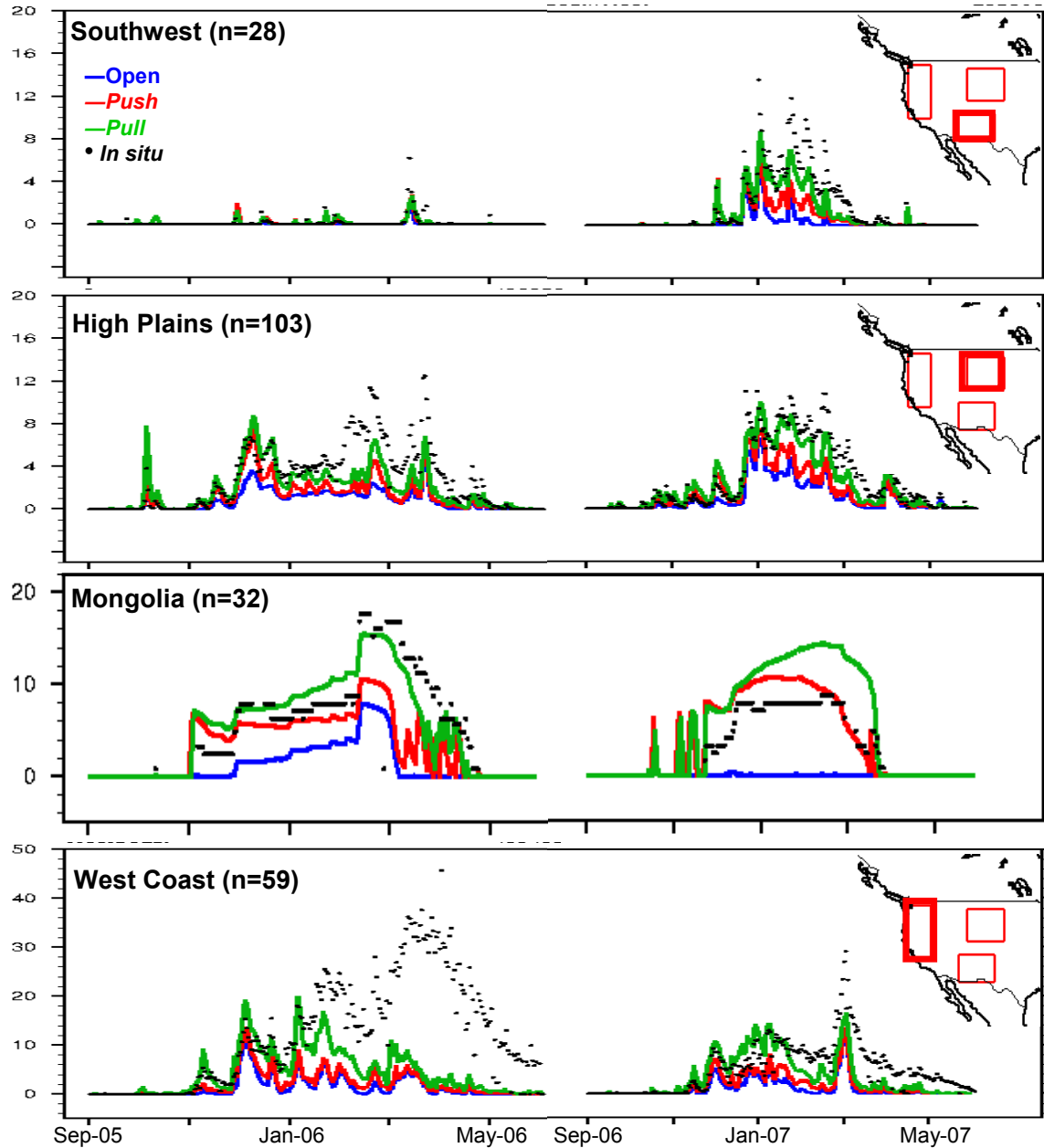
Figure 5: (A) MODIS and Open Loop Noah estimates of SCA for a simulation grid box including Shaver Lake, CA (37.2N, 119.4W). (B-H) Daily open loop, *push*, and *pull* values of (B) SWE, (C) local water balance, (D) accumulated runoff, (E) accumulated snowfall, (F) accumulated rainfall, (G) air temperature, and (H) daily snowmelt for the same location. In panel C, the *pull* simulation falls directly on top of open loop. In panels D-F, the *push* simulation is identical to open loop.
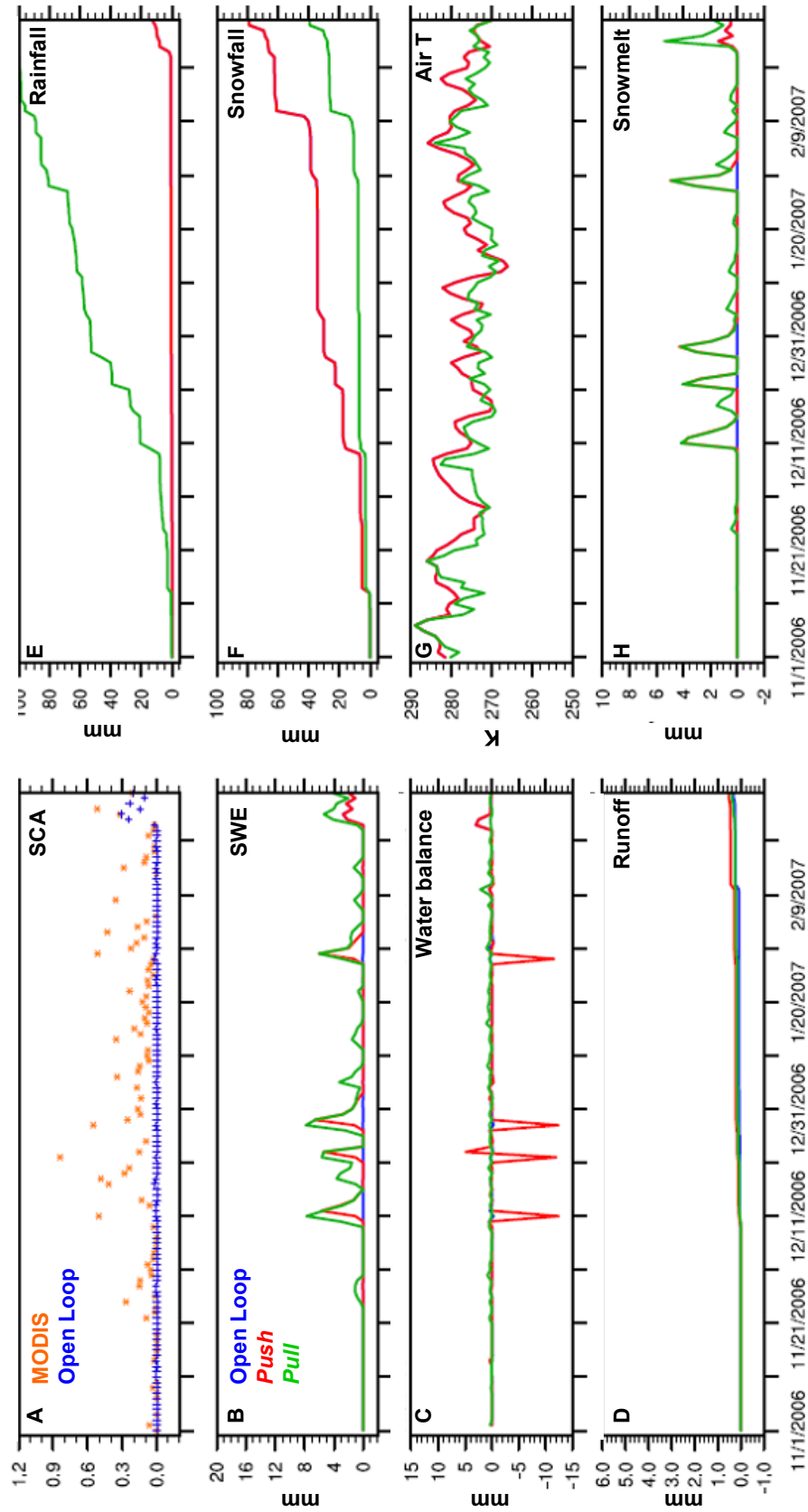
Figure 6: As in Figure 5, for a Russian Site near Lensk, 300km N of Lake Baikal (58.7N, 108.7E)
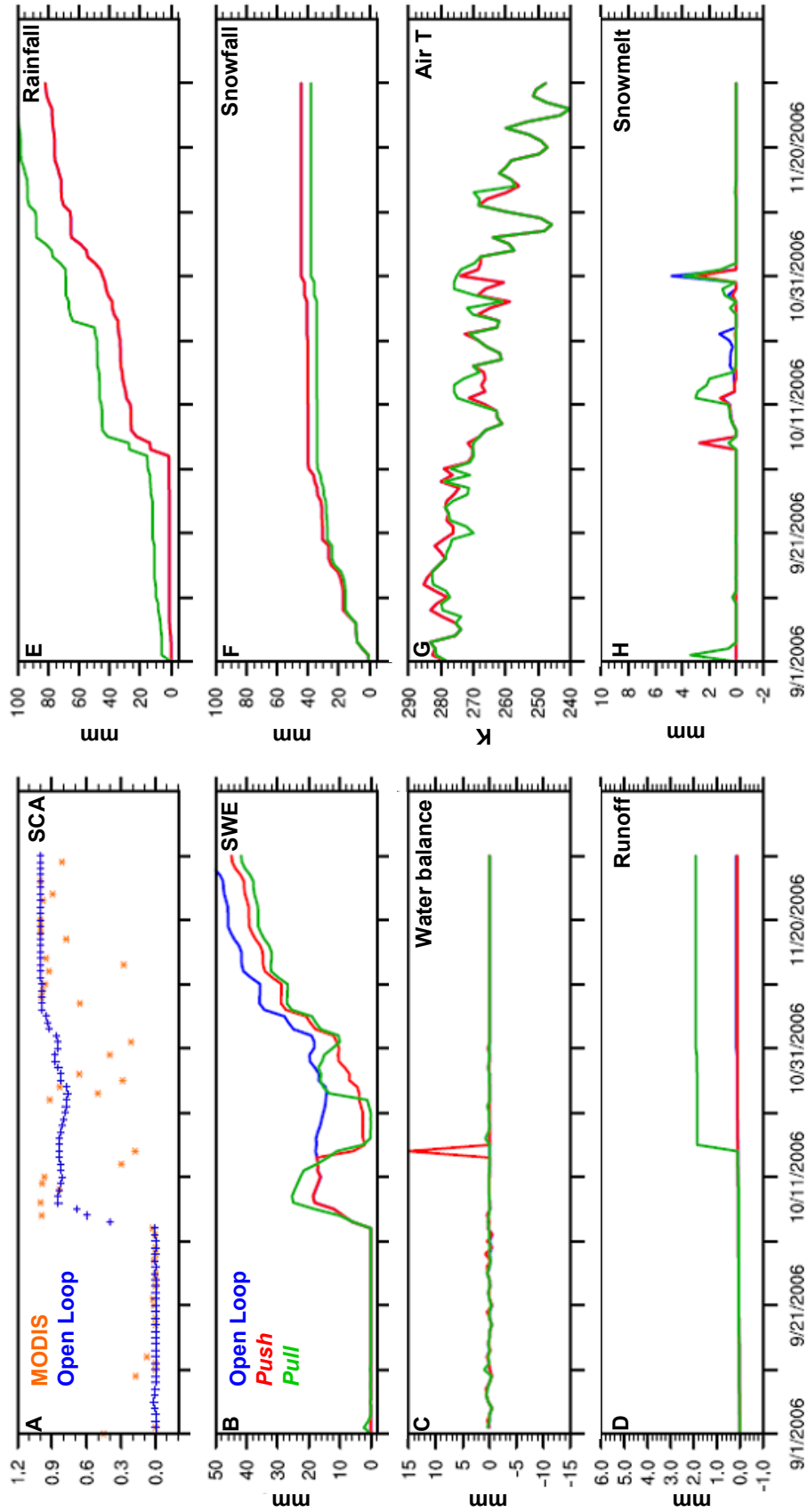
Figure 7: As in Figure 5, for a location near Moriarty, New Mexico (35.1N, 105.8W).